

# Quasi-Equatorial Gravitational Lensing by Spinning Black Holes in the Strong Field Limit

V. Bozza

Dipartimento di Fisica "E.R. Caianiello", Università di Salerno, Italy.  
Istituto Nazionale di Fisica Nucleare, Sezione di Napoli.

(Dated: February 8, 2020)

We calculate the pattern of relativistic images of a given source, generated by a spinning black hole. In this work we are mainly interested to trajectories lying on the equatorial plane. Images formed by photons winding in the sense of rotation of the black hole appear closer to the center, while photons winding in the opposite sense form farther images. When photons travel inside the ergosphere, the properties of the images drastically change. We also extend our treatment to quasi-equatorial motion, describing the precession of the orbits and writing a two-dimensional lens equation. We then calculate the critical points, the caustics and the magnification on the equatorial plane. The caustics acquire a finite extension, covering several Riemann folds for high angular momenta. The whole analysis is carried out in the strong field limit.

PACS numbers: 95.30.Sf, 04.70.Bw, 98.62.Sb

Keywords: Relativity and gravitation; Classical black holes; Gravitational lensing

## I. INTRODUCTION

Gravitational lensing, since its beginning, has been used to test General Relativity in the weak field approximation. Later on, several studies of null geodesics in strong gravitational fields have been lead in past years. Bardeen et al. [1] studied the appearance of a black hole in front of a uniform source; Viegutz [2] made a semi-analytical investigation of null geodesics in Kerr geometry; Nemiro [3] studied the visual distortions around a neutron star and around a black hole; Falcke, Melia & Agol [4] considered the luminosity of the accretion flow as a source.

A recent paper by Virbhadra & Ellis [5] has risen a new interest about gravitational lensing as a probe for strong gravitational fields generated by collapsed objects, providing a new important test for the full general relativity. They have shown that a source behind a Schwarzschild black hole would generate an infinite series of images on both sides of the lens. These relativistic images are formed by light rays passing close to the event horizon and winding several times around the black hole before emerging towards the observer. By an alternative formulation, Frittelli, Kling & Newman [6] attained an exact lens equation, giving integral expressions for its solutions, and compared their results to those by Virbhadra & Ellis. The phenomenology of collapsed objects with naked singularities, analysed by Virbhadra & Ellis in another work [7], is radically different. This difference provides a possible way to test the correctness of the cosmic censorship conjecture.

A new, simple and reliable method to investigate the subject was proposed by Bozza et al. in Ref. [8]. They revisited the Schwarzschild black hole lensing defining a

strong field limit for the deflection angle, which retained the first two leading order terms. By this approximation, a fully analytical treatment was developed and simple formulae for the position and the magnification of the images were derived. The same method was applied by Eiroa, Romero & Torres [9] to a Reissner-Nordstrom black hole, confirming the appearance of a similar pattern of images. Later on, the formulae given in Ref. [8] were used by Petters [10] to calculate relativistic effects on microlensing events. Finally, in a previous work, we have developed a generalization of the strong field limit to an arbitrary spherically symmetric spacetime [11], comparing the image patterns for several interesting metrics. We have shown that different collapsed objects are distinguishable by a careful examination of the separation between the first two relativistic images and their luminosity ratio. The sensitivities required for such measures are out of the actual VLBI projects [12], but might be reached in a not so far future.

Insofar, only spherically symmetric black holes have been adequately investigated. Yet, in general, a black hole would be characterized by a non-zero angular momentum which breaks spherical symmetry, leaving only a rotational symmetry around one axis. Rotation heavily affects the gravitational field around the collapsed object. It is thus natural to expect relevant modifications in the phenomenology of strong field gravitational lensing. However, the loss of the spherical symmetry is a major obstacle for any calculations.

Previous works on the subject have selected the supermassive black hole hosted by the radio source Sagittarius A\* [13] as the best candidate for strong field gravitational lensing [5, 11]. Its mass has been estimated to be  $M = 2.6 \cdot 10^6 M_{\odot}$  but our knowledge on a possible intrinsic angular momentum of this object is still very poor. However, the analysis of the variability of the spectrum in the mm-submm region suggests the possibility of a

---

Electronic address: valbozza@sa.infn.it

non-negligible spin [14]. In particular, the value

$$|a| \approx 0.088 \quad (1)$$

has been proposed, but high uncertainties in the assumptions behind the calculations may push the spin towards even higher values.

The purpose of this paper is to investigate the relevance of the black hole spin in strong field lensing phenomenology. We formulate the strong field limit for Kerr black hole lensing, considering trajectories close to the equatorial plane. With this limitation we cannot give a complete description of the whole phenomenology, which we shall delay to future works. However, as we shall see, quasi-equatorial motion gives very important indications which are very useful to understand also the general case. In Sect. 2 we recall some general properties of Kerr geodesics. In Sect. 3 we carry out the strong field limit expansion of the deflection angle on the equatorial plane in a Kerr geometry. In Sect. 4 we move off from the equatorial plane and consider trajectories at small declinations. In Sect. 5 we write the lens equation on the equatorial plane. In Sect. 6 we write a polar lens equation dealing with displacements normal to the equatorial plane. In Sect. 7 we find the positions of the caustic points and the magnification of all images. Sect. 8 contains the summary.

## II. GEODESICS IN KERR SPACETIME

In Boyer-Lindquist coordinates [15], the Kerr metric reads

$$ds^2 = \frac{a^2 \sin^2 \theta}{2} dt^2 - dx^2 - r^2 d\theta^2 - \frac{x^2 + a^2 - a^2 \sin^2 \theta}{2} \sin^2 \theta d\phi^2 + \frac{2ax \sin^2 \theta}{2} dt d\phi \quad (2)$$

$$= x^2 - x + a^2 \quad (3)$$

$$r^2 = x^2 + a^2 \cos^2 \theta \quad (4)$$

where  $a$  is the specific angular momentum of the black hole. All distances are measured in Schwarzschild radii ( $\frac{2M}{c^2} = 1$ ).

The Kerr space is characterized by a spherical event horizon at  $x_H = \frac{1 + \sqrt{1 - 4a^2}}{2}$  for  $|a| < 0.5$ . Beyond this critical value there is no event horizon and causality violations are present in the whole spacetime, with the appearance of a naked singularity [16, 17]. We shall restrict to subcritical angular momenta. The ellipsoid

$a^2 \sin^2 \theta = 0$  is the static limit bounding the region where every static worldline ( $\dot{x} = \dot{\theta} = \dot{\phi} = 0$ ) becomes spacelike. The region between the static limit and the horizon is called ergosphere: here everything is bound to rotate around the black hole.

The geodesics equations can be derived taking

$$L = g \frac{dx}{ds} \frac{dx}{ds} \quad (5)$$

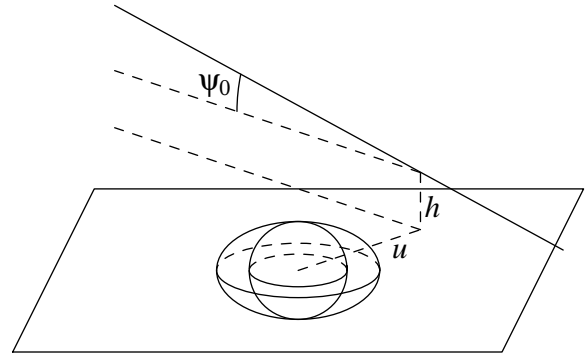


FIG. 1: The three parameters identifying an incoming light ray.

as the Lagrangian.

In general, we can identify a light ray coming from infinity by three parameters (Fig. 1). If there were no gravitational field, a photon would proceed on a straight line. Its projection on the equatorial plane would reach a minimum distance  $u$ , which we shall call the projected impact parameter. At this minimum projected distance, the light ray would have some height  $h$  on the equatorial plane. Finally, the inclination  $\psi_0$  is the angle that the light ray would form with the equatorial plane. When we switch on the gravitational field, the light ray is obviously deviated from this ideal straight line, but these three parameters can still be used to label any light ray coming from infinity.

Two constants of motion are the energy and the angular momentum of the particle, given by

$$2E = \frac{\partial L}{\partial t} \quad (6)$$

$$2J = \frac{\partial L}{\partial \phi} \quad (7)$$

By a suitable choice of the affine parameter, we set

$$E = 1 \quad (8)$$

and write the angular momentum in terms of the initial conditions

$$J = u \cos \psi_0; \quad (9)$$

From Eqs. (6)–(7), we find an expression for  $\frac{dt}{ds}$  and  $\frac{d\phi}{ds}$  in terms of  $x$ ,  $\theta$  and the initial conditions.  $L$  is another constant of motion, which vanishes for null geodesics and can be used to write  $\frac{dx}{ds}$ . Finally,  $\frac{d\theta}{ds}$  can be obtained in terms of a fourth integral of motion, separating the Hamilton-Jacobi equation [16]:

$$2 \frac{d\theta}{ds} = \sqrt{Q} = \sqrt{a^2 \cos^2 \theta + J^2 \cot^2 \theta} \quad (10)$$

The integral of motion  $Q$  can be expressed in terms of the initial conditions as

$$Q = h^2 \cos^2 \psi_0 + (u^2 - a^2) \sin^2 \psi_0 \quad (11)$$

In this way, the geodesics equations are reduced to four first order differential equations, suitable for a detailed study.

### III. DEFLECTION ANGLE IN THE EQUATORIAL PLANE

In this section, we consider light rays lying on the equatorial plane  $\theta = \frac{\pi}{2}$  by setting  $h = \theta = 0$ . The reduced metric has the form

$$ds^2 = A(x)dt^2 - B(x)dx^2 - C(x)d\phi^2 + D(x)d\tau^2 : (12)$$

with

$$\begin{aligned} A(x) &= 1 - \frac{1}{x} \\ B(x) &= \frac{1}{1 - \frac{1}{x} + \frac{a^2}{x^2}} \\ C(x) &= x^2 + a^2 + \frac{a^2}{x^2} \\ D(x) &= 2\frac{a}{x} \end{aligned} \quad (13)$$

What we say in this section is immediately extendable to any axially symmetric spacetime if we replace Eq. (13) by any other expression.

As  $\theta = 0$ , by Eq. (9) the angular momentum  $J$  coincides with the impact parameter  $u$ . In general, a light ray coming from infinity will approach the black hole, reach a minimum distance  $x_0$  and then leave again towards infinity. Evaluating the Lagrangian at  $x = x_0$ , we find an implicit relation between  $J = u$  and the closest approach distance  $x_0$

$$J = u = \frac{D_0 + \sqrt{4A_0C_0 + D_0^2}}{2A_0}; \quad (14)$$

where all the functions with the subscript 0 are evaluated at  $x = x_0$ . The impact parameter  $u$  is then univocally determined by  $x_0$  and vice versa. Choosing the positive sign before the square root, we describe only light rays winding counterclockwise when seen from above. For  $a > 0$  the black hole also rotates counterclockwise, while for  $a < 0$  the black hole and the photon rotate in opposite senses.

From Eq. (12), using also the expression of  $\frac{d\phi}{ds}$ , we find the angular shift as a function of the distance

$$\frac{d\phi}{dx} = P_1(x; x_0)P_2(x; x_0) \quad (15)$$

$$P_1(x; x_0) = \frac{1}{\sqrt{C A_0}} \frac{1}{\sqrt{4AC + D^2}} \quad (16)$$

$$P_2(x; x_0) = \frac{1}{A_0} \frac{1}{\sqrt{A \frac{C_0}{C} + \frac{J}{C} (AD_0 - A_0D)}} \quad (17)$$

Integrating this expression from  $x_0$  to infinity we find half the deflection angle as a function of the closest ap-

proach. Given the symmetry between approach and departure, we can write

$$\alpha(x_0) = \int_{x_0}^{\infty} \frac{d\phi}{dx} dx \quad (18)$$

$$\alpha(x_0) = 2 \int_{x_0}^{\infty} \frac{d\phi}{dx} dx \quad (19)$$

The expression for a spherically symmetric metric, given in Ref. [11] can be recovered setting  $D = D_0 = 0$  and  $J = \frac{C_0}{A_0}$ .

The deflection angle grows as  $x_0$  decreases. It diverges when  $x_0$  reaches a minimum value  $x_m$  which represents the radius of the photon sphere. If a photon falls inside this sphere, it is destined to be absorbed by the black hole. Of course, we will have different photon spheres for photons winding in the same sense of the rotation of the black hole (hereafter left-winding photons) and for photons winding in the opposite sense (right-winding). In general, we expect the latter to be absorbed more easily. Their photon sphere will thus be larger than that of left-winding photons, which can escape more easily. As we shall see later, this is what happens.

Following the philosophy of the strong field limit, we look for an expansion of the deflection angle of the form

$$\alpha(x_0) = \bar{a} \log \frac{D_{0L}}{u_m} + \bar{b} + O(u - u_m) \quad (20)$$

where the coefficients  $u_m$ ,  $\bar{a}$  and  $\bar{b}$  depend on the metric functions evaluated at  $x_m$ .  $D_{0L}$  is the distance between the lens and the observer, so that the angular separation of the image from the lens is  $\theta = \frac{u}{D_{0L}}$ .

All the steps to be taken towards this final expression are very similar to those of Ref. [11], with few adjustments. We shall sketch them very briefly.

We define the variables

$$y = A(x) \quad (21)$$

$$z = \frac{y - y_0}{1 - y_0} \quad (22)$$

where  $y_0 = A_0$ . The integral (19) in the deflection angle becomes

$$\alpha(x_0) = \int_{z_0}^1 R(z; x_0) f(z; x_0) dz \quad (23)$$

$$R(z; x_0) = 2 \frac{1 - y_0}{A_0(x)} P_1(x; x_0) \quad (24)$$

$$f(z; x_0) = P_2(x; x_0) \quad (25)$$

where  $x = A^{-1}[(1 - y_0)z + y_0]$ .

The function  $R(z; x_0)$  is regular for all values of  $z$  and  $x_0$ , while  $f(z; x_0)$  diverges for  $z \rightarrow 0$ . To find out the order of divergence of the integrand, we expand the argument of the square root in  $f(z; x_0)$  to the second order in  $z$

$$f(z; x_0) \approx f_0(z; x_0) = \frac{1}{\sqrt{z + \frac{z^2}{2}}} : \quad (26)$$

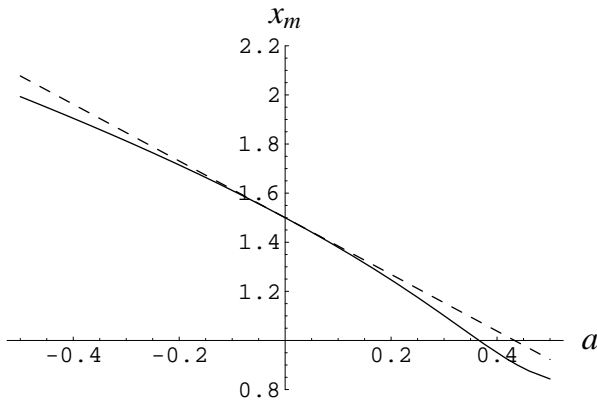


FIG. 2: The radius of the photon sphere versus the black hole angular momentum. The solid line is the numerical solution, the dashed one is the linear approximation.

When  $\epsilon$  is non zero, the leading order of the divergence in  $f_0$  is  $z^{-1/2}$ , which can be integrated to give a finite result. When  $\epsilon$  vanishes, the divergence is  $z^{-1}$  which makes the integral diverge. Then the outermost solution of the Eq.  $\Delta = 0$  defines the radius of the photon sphere  $x_m$  (see also [18]).

In the case of the Kerr metric, we have

$$\begin{aligned} &= x_0^4 (3 - 5x_0 + 2x_0^2) - a^2 (1 - 3x_0 + 3x_0^2 + x_0^3) + \\ &+ 2ax_0^{3/2} \frac{q}{(x_0 - 1)x_0^4 + a^2(1 + 2x_0 - x_0^2 + x_0^3)} \\ &x_0(x_0 - 1)(x_0^4 + a^2(x_0^2 + 1))^{-1} \end{aligned} \quad (27)$$

which can be solved numerically for any value of the black hole angular momentum. Fig. 2 shows a plot of the radius of the photon sphere as a function of  $a$ . The solution is very well approximated by a linear expansion for low angular momenta

$$x_m \approx \frac{3}{2} - \frac{2a}{3} \quad (28)$$

As expected, for positive angular momenta, (left-winding) photons are allowed to get closer to the black hole, entering even the ergosphere ( $x_m$  falls below 1) at high values of  $a$ . It is possible to calculate exactly from Eq.  $\Delta = 0$  at what angular momentum this happens. The critical value is

$$a_{cr} = \frac{1}{1 + \frac{1}{3}} = 0.366 \quad (29)$$

For negative angular momenta, (right-winding) light rays must keep farther from the center.

The procedure to find the strong field limit coefficients is from now on identical to that described in Ref. [11], with  $R(z; x_0)$ ,  $f(z; x_0)$  and  $f'(z; x_0)$  given by Eqs. (24), (25) and (26), respectively. We shall not repeat the whole technique here but just specify the results of Ref. [11] for our metric.

The strong field limit coefficients of the expansion (20) are

$$u_m = \frac{D_m + \frac{P}{4A_m C_m + D_m^2}}{2A_m} \quad (30)$$

$$\bar{a} = \frac{R(0; x_m)}{2 \frac{P}{m}} \quad (31)$$

$$\bar{b} = b_D + b_R + \bar{a} \log \frac{c x_m^2}{u_m} \quad (32)$$

where

$$b_D = 2\bar{a} \log \frac{2(1 - y_m)}{A_m^0 x_m} \quad (33)$$

$z^1$

$$b_R = \int_0^1 [R(z; x_m) f'(z; x_m) - R(0; x_m) f_0'(z; x_m)] dz \quad (34)$$

and  $c$  is defined by the expansion

$$u = u_m = c(x_0 - x_m)^2 \quad (35)$$

All the functions with the subscript  $m$  are evaluated at  $x_0 = x_m$ .

Fig. 3 shows the strong field limit coefficients as functions of  $a$ .  $u_m$  decreases with  $a$ , while  $\bar{a}$  and  $\bar{b}$  grow together until the photon sphere falls inside the ergosphere. Then, if the photon spends enough time in this region, surprisingly they start to decrease. As a consequence of this inversion, the images appear more packed and the magnification decreases as we will see in detail in Sect. V II.

#### IV. PRECESSION OF THE ORBITS AT SMALL DECLINATIONS

The study of the deflection angle for photons lying on the equatorial plane is sufficient to write a one-dimensional lens equation. However, to address the caustic structure and calculate the magnification of the images, we need a two-dimensional lens equation. For this reason, in this section we analyze trajectories close to the equatorial plane. They are described by one further coordinate, which is the polar angle  $\theta$ . The problem becomes too involved to be solved in general but we shall give a complete description for quasi-equatorial motion, preserving also the simplicity and immediacy of the strong field limit scheme.

In order to remain at small latitudes, we restrict to light rays characterized by a small inward inclination  $\theta_0$  and small height  $h$  compared to the projected impact parameter  $u$ , with  $\theta_0 \approx \frac{h}{u}$ . Retaining the first relevant terms, from Eqs. (9)–(11) we get

$$J' = u \quad (36)$$

$$Q' = h^2 + \frac{\bar{u}^2}{P} \frac{2}{u} \quad (37)$$

$$\bar{u} = \frac{u^2}{a^2} \quad (38)$$

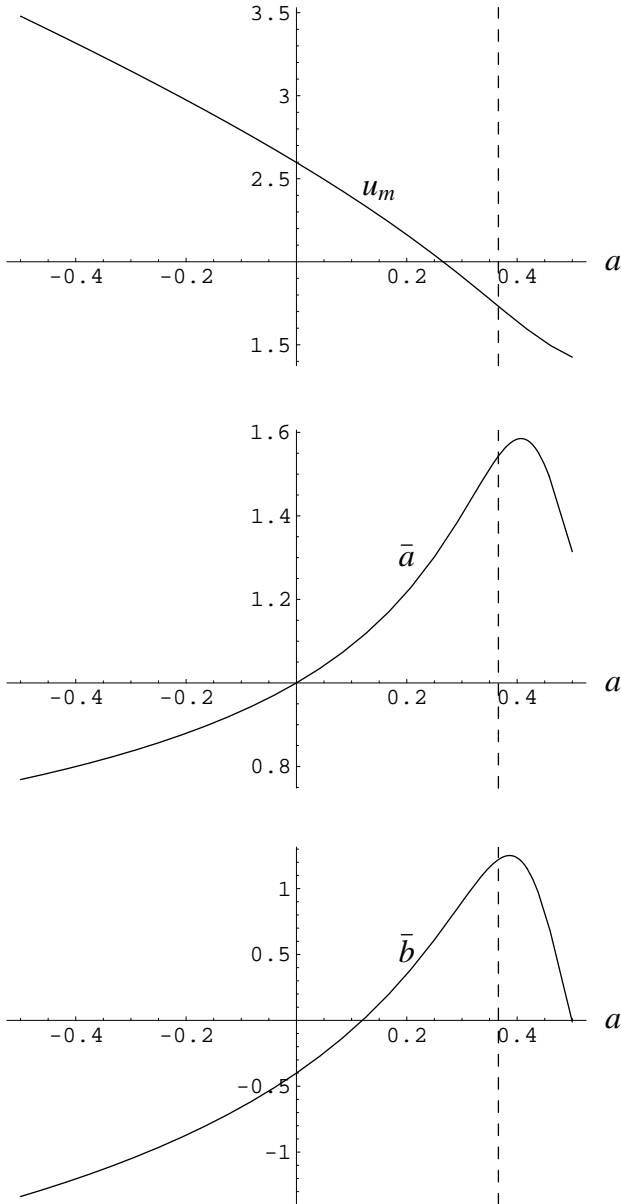


FIG. 3: Coefficients of the strong field limit versus black hole angular momentum. For angular momenta beyond  $\frac{1}{1+\sqrt{3}}$ , marked by the dashed vertical line, the photon sphere falls inside the ergosphere.

We require the declination  $\theta = \frac{\pi}{2} \pm \delta$  to stay small (of the order of  $\delta_0$ ) during the motion. Dividing Eq. (10) by  $\frac{d}{ds}$ , we get a simple evolution equation for  $\delta$  as a function of the azimuth

$$\frac{d\delta}{d\phi} = \delta \left( \frac{q}{r^2} - \frac{1}{2} \right) \quad (39)$$

with

$$q = \frac{r}{\bar{u}^2} + \frac{2}{r_0} \quad (40)$$

$$!(\phi) = \bar{u} \frac{a^2 + x(\phi)(x(\phi) - 1)}{[a + u(x(\phi) - 1)]x(\phi)} \quad (41)$$

In the Schwarzschild case ( $a = 0$ ),  $! = 1$  and Eq. (39) is immediately solved to

$$!(\phi) = \bar{u} \cos(\phi + \phi_0) \quad (42)$$

After each loop around the black hole, the declination returns to the initial value. This means that there is no precession of the orbital plane, as expected for a spherically symmetric black hole.

For non-vanishing angular momenta,  $!$  is no longer a constant, since  $x$  depends on  $\phi$ , and Eq. (39) cannot be solved analytically. However, it is easy to approximate  $!(\phi)$  by a simple polynomial function once we understand its behaviour. We know that the photon comes from  $x = 1$  and finally returns to infinity, so that

$$!(0) = !(\phi_f) = !_1 \quad \frac{\bar{u}}{u} \quad (43)$$

We also know that  $!(\phi)$  is symmetric before and after  $\phi = \phi_f/2$ , which is the azimuth when the minimum distance  $x_0$  is reached by the photon. Here, we have

$$! \left( \frac{\phi_f}{2} \right) = !_0 = \bar{u} \frac{a^2 + x_0(x_0 - 1)}{(a + u(x_0 - 1))x_0} \quad (44)$$

$!_0$  is typically smaller than  $!_1$  when  $a > 0$  and higher when  $a < 0$ . Then  $!(\phi)$  starts from  $!_1$ , decreases (increases) to its minimum (maximum)  $!_0$  at  $\phi = \phi_f/2$  and then increases (decreases) back reaching again the initial value at  $\phi_f$ .

Moreover, we can calculate the derivative of  $!(\phi)$  in  $\phi = 0$

$$\frac{d!}{d\phi} = \frac{d!}{dx} \frac{dx}{d\phi} \quad (45)$$

recalling that  $\frac{dx}{d\phi}$  is known from Eq. (15). Evaluating at  $\phi = 0$ ,  $x = 1$ , we get  $!_1' = !_1'(0)$ . In principle it is possible to calculate derivatives of arbitrary order in  $\phi = 0$  iterating the procedure. In this way, we can approximate  $!$  with an arbitrary accuracy. However, we stop here and write a quartic polynomial for  $!(\phi)$

$$!(\phi) = !_0 + c_2 \frac{\phi^2}{f} + c_4 \frac{\phi^4}{f} \quad (46)$$

and determine  $c_2$  and  $c_4$  matching with  $!$  and  $!_1'$  at  $\phi = 0$ . This is sufficient to illustrate the whole phenomenology and obtain realistic results saving the simplicity of the analytic construction. Anyway, a higher precision can be attained simply increasing the order of the polynomial and involving higher order derivatives in  $\phi = 0$ .

Once we have a manageable expression for  $\bar{\delta}(\theta)$ , Eq. (39) can be integrated immediately in the general case to give

$$\bar{\delta}(\theta) = \bar{\delta}_0 \cos \theta + \delta_1 \theta \quad (47)$$

with

$$\bar{\delta}_0 = \int_0^{\theta} \bar{\delta}(\theta') d\theta' \quad (48)$$

Having approximated  $\bar{\delta}(\theta)$  by a polynomial, this integral is trivial and the problem is completely solved.

As a general remark, we can say that for positive angular momenta  $\bar{\delta}$  is always less than one. As the photon approaches the black hole,  $\bar{\delta}$  decreases further and the orbital plane suffers a counterclockwise precession, i.e. after each loop it is necessary an additional  $\theta$  to reach the same declination  $\delta$ . On the contrary, for negative angular momenta,  $\bar{\delta}$  starts from  $\bar{\delta}_1 < 1$  but becomes greater than one as the photon approaches the black hole. In this case, the precession is clockwise, i.e. the photon reaches the same declination before completing a loop.

The integration constant  $\delta_0$  in Eq. (47) is fixed by the initial conditions. In particular, we have to impose that at  $\theta = 0$  the declination is just minus the inclination of the incoming photon trajectory, that we have indicated by  $\theta_0$ . The result is that

$$\delta_0 = \text{Sign}[h] \arccos \frac{\theta_0}{\bar{\delta}} \quad (49)$$

The declination of the outward photon is thus

$$\delta_f(\theta_f) = \bar{\delta} \cos \theta_f + \delta_0 \quad (50)$$

In alternative, using the expression of  $\delta_0$ , we can write

$$\delta_f = \delta_0 \cos \theta_f + \frac{h}{u} \sin \theta_f \quad (51)$$

The phase  $\bar{\delta}_f$  is

$$\bar{\delta}_f = \int_0^{\theta_f} \bar{\delta}(\theta) d\theta = \frac{f}{30} (14!_1 + 16!_0 + !_1^0 \theta_f) \quad (52)$$

in our quartic approximation. This quantity has a central importance in the discussion of Sects. VI, VII.

## V. LENSING IN THE EQUATORIAL PLANE

Let us start from the ideal case when observer and source both lie on the equatorial plane of the Kerr black hole. The whole trajectory of the photon is then confined on the same plane.

In previous works, the strong field limit has been developed assuming an almost perfect alignment of source,

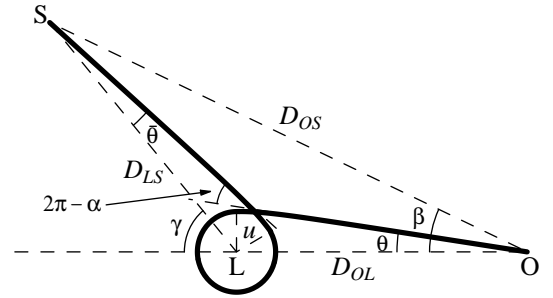


FIG. 4: The lensing geometry projected on the equatorial plane in the case of the first relativistic image.  $\alpha$  is the angular separation between the image and the lens as seen by the observer,  $\beta$  is the angular position of the source as seen by the observer,  $\gamma = \frac{u}{D_{LS}} = \frac{D_{OL}}{D_{LS}}$ .

lens and observer. This because, for spherically symmetric metrics, the better the alignment the higher is the magnification. As we shall see in Sec. VII, this is no longer the case for Kerr black holes. Therefore we shall write the equatorial lens equation in a more general way.

The optical axis is the line joining the observer and the lens. Setting the origin on the black hole, the angle between the direction of the source and the optical axis will be indicated by  $\theta$ .  $\theta = 0$  is the case of an almost perfect alignment discussed in Refs. [8, 9, 10, 11]. From the lensing geometry, illustrated in Fig. 4, we can write the relation

$$\sin \theta = \frac{D_{OL}}{D_{OS}} \sin \alpha + \frac{D_{LS}}{D_{OS}} \sin \beta \quad (53)$$

where

$$\sin \theta = \frac{u}{D_{LS}}, \quad \frac{D_{OL}}{D_{LS}} \quad (54)$$

and  $D_{LS}$  is the distance between the lens and the source.

The equatorial lens equation is

$$\sin \theta = \frac{D_{OL} + D_{LS}}{D_{LS}} \sin \alpha \quad (\theta) \text{ mod } 2 \quad (55)$$

In this lens equation  $\theta$  can assume any value in the trigonometric interval  $[\theta; \theta + \pi]$ . The source may even be on the same side of the observer when  $\theta = 0$ . The relation between  $\theta$  and  $\alpha$  (the angular position of the source as seen by the observer) is

$$\sin \theta = \frac{D_{LS}}{D_{OS}} \sin \alpha \quad (56)$$

but here in general we cannot substitute the sines by their arguments.  $D_{OS}$  is the distance between source and observer which is different from the distance covered by lensed photons  $D_{OL} + D_{LS}$ .

To solve the lens equation, since  $\beta \ll 1$ , in a first step we solve the Eq.  $\beta = \beta(\alpha) \bmod 2\pi$ , to find

$$\beta_n^0 = \frac{u_m}{D_{OL}} (1 + e_n) \quad (57)$$

$$e_n = e^{\frac{2\pi n}{a}}; \quad (58)$$

where  $n = 1; 2; \dots$  indicates the number of loops done by the photon around the black hole. This solution is then corrected expanding  $\beta(\alpha)$  around  $\beta_n^0$

$$\beta(\alpha) = \beta_n^0 + \frac{\partial \beta}{\partial \alpha}(\beta_n^0) (\alpha - \alpha_n^0) + o(\alpha - \alpha_n^0), \quad (59)$$

Substituting in (55) and neglecting higher order terms, we find

$$\beta_n^0 \approx \beta_n^0 \left( 1 - \frac{u_m e_n (D_{OL} + D_{LS})}{\bar{a} D_{OL} D_{LS}} \right); \quad (60)$$

where the correction is much smaller than  $\beta_n^0$ .

Images are formed on both sides of the lens. As all strong field limit coefficients depend on  $a$  we have to be careful and choose the correct sign for the angular momentum. Conventionally we call north the direction of the black hole spin. Then photons winding counterclockwise are left-winding and are described by a positive  $a$ . They form images on the eastern side of the black hole. Images formed by right-winding rays appear on the western side and are described taking a negative  $a$  and reversing the sign of  $\beta$ .

## VI. LENSING AT SMALL DECLINATIONS

The lens equation (55) describes trajectories lying on the equatorial plane and can be employed to calculate the positions of the relativistic images. However, to investigate the problem on a deeper level we are forced to study what happens at least for small displacements from the equatorial plane. We shall assist Eq. (55) by its polar counterpart, describe the caustic structure, compute the magnification and have a precise idea of what happens in the general case.

Thanks to the small declination hypothesis, at the lowest order we can neglect any backreaction on the equatorial lens equation. In all our discussion we shall speak as if the photon were emitted by the observer and absorbed by the source. Of course there is no difference in which direction we let the photon travel on its trajectory (apart from the sign of  $a$  which must be chosen correctly).

Consider a source whose height on the equatorial plane is  $h_S$ . The height of the observer will be indicated by  $h_O$ . We shall assume  $u = (h_O; h_S) = (D_{OL}; D_{LS})$  (see Fig. 5). Recalling the meaning of the parameters  $\beta_0$  and  $h$

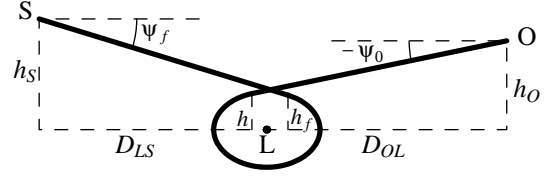


FIG. 5: The lensing geometry projected on the vertical plane. In this picture we have assumed  $\beta = 0$  for simplicity.

used insofar to identify the incoming light ray, we can write down the simple geometric relation

$$h = h_O + D_{OL} \beta_0; \quad (61)$$

A similar relation holds between the outgoing photon parameters  $h_f$ ,  $\beta_f$  and the source position

$$h_S = h_f + D_{LS} \beta_f; \quad (62)$$

Given the positions of source and observer, our purpose is to determine  $\beta_0$ , the inclination under which the observer emits (sees) the light ray.

By symmetry between the outgoing and the incoming parameters, Eq. (40) for  $\beta_0$  can be written substituting  $\beta_0$  and  $h$  by  $\beta_f$  and  $h_f$

$$\beta_0 = \frac{h_f}{\bar{u}} \sin \beta_f + \beta_f; \quad (63)$$

In this way, we can express  $h_f$  in terms of  $\beta_f$  and then, by Eq. (50), in terms of  $\beta_f$  and  $\beta_0$

$$h_f = \text{Sign}[h_f] \bar{u} \sin \beta_f = \bar{u} \sin \beta_f + \beta_0; \quad (64)$$

Recalling Eq. (49), we also get

$$h_f = \bar{u} \sin \beta_f - h \cos \beta_f; \quad (65)$$

Substituting in Eq. (62) together with Eq. (51), we get

$$h_S = \beta_0 \bar{u} S - h C - D_{LS} \beta_0 C + D_{LS} \frac{h}{\bar{u}} S; \quad (66)$$

where

$$S = \sin \beta_f; \quad (67)$$

$$C = \cos \beta_f; \quad (68)$$

Finally, substituting  $h$  from Eq. (61) and discarding higher order terms, we obtain the lens equation in the polar direction

$$h_S = h_O \frac{D_{LS}}{\bar{u}} S - C \beta_0 (D_{OL} + D_{LS}) C - \frac{D_{OL} D_{LS}}{\bar{u}} S \beta_0; \quad (69)$$

In this equation  $\phi_0$  is directly related to the heights of the observer and the source. The solution is

$$\phi_{0;n} = \frac{h_s + h_0 C_n - h_b \frac{D_{LS}}{u} S_n}{(D_{OL} + D_{LS}) C_n + \frac{D_{OL} D_{LS}}{u} S_n}; \quad (70)$$

where  $S_n$  and  $C_n$  are  $S$  and  $C$  calculated for  $\bar{\phi} = \bar{\phi}_{f;n}$ . The phase  $\bar{\phi}_{f;n}$  of the  $n$ -th image is the only quantity that needs to be calculated preliminarily. However, once the equatorial lens equation (55) is solved, we know the total deflection angle  $\alpha_n$  for the  $n$ -th image and then  $\bar{\phi}_{f;n} = \alpha_n + \phi_0$ . The closest approach  $x_{0;n}$  is related to the impact parameter by Eq. (35). We can then construct  $\bar{\phi}(\phi)$  to the required precision and calculate  $\bar{\phi}_{f;n}$  for each image.

As a consistency check we can see what we obtain in the Schwarzschild case when the photon completes just one loop around the black hole, exiting on the opposite side. In this case  $a = 0$  and  $\bar{\phi}_{f;n} = (2n + 1)\pi$ . We get

$$j_{\bar{\phi} = (2n+1)\pi} = \frac{h_s - h_b}{D_{OL} + D_{LS}}; \quad (71)$$

which is the correct result for photons passing very close to the black hole, looping around it.

The consistency of our approximation requires that  $\phi_0 \ll 1$  and  $h \ll u$ . From Eq. (61) the height is

$$h_n = \frac{h_s D_{OL} - h_b D_{LS} C_n}{(D_{OL} + D_{LS}) C_n + \frac{D_{OL} D_{LS}}{u} S_n}; \quad (72)$$

For a generic  $\bar{\phi}_f$ , both constraints are automatically satisfied, since the second term in the denominators dominates and we have that  $\phi_0 \ll h_b = D_{OL}$  and  $h \ll u h_0 = D_{OL}$ . However, in the neighborhood of  $\bar{\phi}_f = k\pi$  the denominators of the two expressions can vanish, making diverge both quantities. The equation

$$K(\phi) = u(D_{OL} + D_{LS})C - D_{OL}D_{LS}S = 0 \quad (73)$$

defines the positions of the caustic points. In the next section we will discuss this equation in connection with the magnification of the images formed by sources close to the caustic points which we call enhanced images.

Surprisingly, thanks to the dragging phenomenon, the quasi-equatorial motion is nearly always satisfied, except for enhanced images. In this situation the quasi-equatorial motion hypothesis is satisfied only for particular geometric configurations which keep  $\phi_0$  and  $h$  under control. We can understand on a more intuitive ground the distinction between enhanced and not-enhanced images and the formation of caustic points looking at Eq. (51). For not enhanced images,  $\bar{\phi}_f$  is generic. In order to vary  $\bar{\phi}_f$  and match any position of the source, we can vary  $h$ , without touching  $\phi_0$ . In fact, expanding Eq. (70) according to the hierarchy of distances and considering a generic  $\bar{\phi}_{f;n}$ , we get

$$\phi_{0;n}^{re} = \frac{h_0}{D_{OL}} + \frac{D_{OL} h_s - h_b D_{LS} C_n}{D_{LS} D_{OL} S_n} \frac{u}{D_{OL}} + \phi_0 \frac{h_0 u}{D_{OL}^2}; \quad (74)$$

which at the lowest order does not depend on  $h_s$ . Namely, varying  $h_s$ , the variation of  $\phi_{0;n}^{re}$  is completely negligible and sources with different  $h_b$  are mapped very close each other. This fact also causes the magnification to be very low (see Sect. VII).

Enhanced images, on the contrary, by Eq. (73) are characterized by  $\bar{\phi}_{f;n} \approx k\pi$ . Their value of  $\phi_f$  is locked on the same value of  $\phi_0$  (apart from the sign). To match a variation in  $h_s$ , it is necessary to vary  $\phi_0$  considerably. Higher variations in  $\phi_0$  are translated into higher magnification.

## VII. MAGNIFICATION AND CAUSTICS

The magnification is classically defined as the ratio of the angular area element of the image and the corresponding angular area element of the source that the observer would see if there were no lens. The angular area element of the image is

$$d^2 A_I = d\phi d\theta; \quad (75)$$

The distance covered by the photons is  $D_{OL} + D_{LS}$  and then the corresponding angular area element of the source is

$$d^2 A_S = \frac{D_{LS} d\phi dh_s}{(D_{OL} + D_{LS})^2}; \quad (76)$$

In fact the source element in the vertical direction is  $dh_s = (D_{OL} + D_{LS}) d\phi$ . In the horizontal direction, the source element is spanned by  $d\theta$  when seen from the lens which corresponds to an angle  $\frac{D_{LS} d\theta}{D_{OL} + D_{LS}}$  seen from the observer. If we want to compare the luminosity of a lensed image with the luminosity of the direct image (namely the source observed directly along  $D_{OS}$  without lensing), the magnification is to be multiplied by the factor  $\frac{(D_{OL} + D_{LS})^2}{D_{OS}^2}$ .

Our lens application has the form

$$\bar{\phi} = \bar{\phi}(\phi); \quad (77)$$

$$h_s = h_s(\phi; \phi_0); \quad (78)$$

where the dependence on  $\phi$  in the polar lens application is through  $\bar{\phi}_f$  and we have neglected the backreaction of  $\phi_0$  on  $\bar{\phi}_f$ . The ratio between  $d\phi dh_s$  and  $d\phi d\theta$  is given by the modulus of the Jacobian determinant of the lens application

$$j\bar{j} = \frac{\partial \bar{\phi}}{\partial \phi} \frac{\partial h_s}{\partial \theta}; \quad (79)$$

The magnification is then given by

$$\mu = \frac{d^2 A_I}{d^2 A_S} = \frac{(D_{OL} + D_{LS})^2}{D_{LS}} \frac{1}{j\bar{j}}; \quad (80)$$

By the equatorial lens equation (55), retaining the dominant terms, we have

$$\frac{\partial \bar{\phi}}{\partial \phi} \approx \frac{\partial D_{OL}}{\partial u_m e}; \quad (81)$$

with

$$e = e^{\frac{\bar{E}_+}{\bar{a}}}; \quad (82)$$

Here we can assume any negative real value, since  $m$  mod 2 represents the angular position of the source (the former meaning of  $\theta$ ) and  $n = \frac{2m}{2}$  is the number of loops done by the photon. Encompassing the number of loops in  $\theta$ , we can write a unique formula for all the relativistic images.

By the polar lens equation (69), we have

$$\frac{\partial h_S}{\partial \theta_0} = (D_{OL} + D_{LS})C \frac{D_{OL}D_{LS}}{\bar{u}} S; \quad (83)$$

Assembling everything together, we get

$$= \frac{(D_{OL} + D_{LS})^2}{D_{OL}D_{LS}} \frac{\bar{u}u_m e}{\bar{a} \bar{D}_{OL}D_{LS}C} \frac{D_{OL}D_{LS}S}{D_{OL}D_{LS}S}; \quad (84)$$

For a generic  $\bar{f}$ ,  $\bar{f} = 0 \frac{u}{D_{OL}}$ , but for the enhanced images,  $\bar{f}$  may even diverge (formally for point-like sources) when the denominator of Eq. (84) vanishes. The  $\theta$ s where this happens are called caustic points. At the lowest order in  $\frac{u}{D_{OL}}$ , Eq. (73) reduces to

$$\bar{f}'_k; \quad (85)$$

The solutions of this equation determines the angular positions  $\theta_k$  of the caustic points for each  $k$ . To have strong field lensing,  $\bar{f}$  must be sensibly greater than  $\theta$  which is the angular shift for a straight line. Then  $k$  must be at least 2.

Expanding around the caustic points, we have

$$K(\theta)'_k K^0(\theta_k)(\theta - \theta_k(a)) = D_{OL}D_{LS} \theta_k(a) (\theta - \theta_k(a)); \quad (86)$$

To understand the nature of these caustic points, notice that in the Schwarzschild limit  $\theta_k(a) \sim 1$  and  $\theta_k(a) \sim (k-1)$ . So that all the odd caustic points are aligned on the optical axis behind the lens on consecutive Riemann folds and the even ones are aligned before the lens. We can recover the Schwarzschild magnification for the images corresponding to sources behind the lens [8]

$$\begin{aligned} \mu_n^{Sch} &= \frac{(D_{OL} + D_{LS})^2}{D_{OL}D_{LS}} \frac{u u_m e_n}{\bar{a} \bar{D}_{OL}D_{LS} (2n-1)j} = \\ &= \frac{D_{OS}}{D_{OL}^2 D_{LS}} \frac{u_m^2 e_n (1 + e_n)}{j j}; \end{aligned} \quad (87)$$

In Fig. 6 we plot the positions of the first five relativistic caustic points as functions of the black hole angular momentum. The first relativistic caustic point is obtained when the photon turns around the black hole and comes back towards the observer.  $\theta_2$  is thus close to  $\theta$  but is anticipated for negative  $a$  and delayed for positive  $a$ .  $\theta_3$  is the first relativistic caustic point with

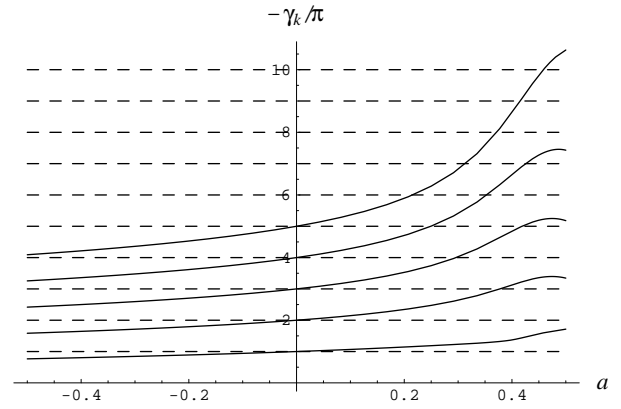


FIG. 6: The angular positions of the first five caustic points:  $k = 2; 3; 4; 5; 6$  from below to above. When  $\theta = 2m$  the source is behind the lens, when  $\theta = (2m + 1)$  the source is before the lens.

a source behind the lens. However, at large angular momenta,  $\theta_3$  becomes lower than  $\theta$  and the source is again before the lens. In Schwarzschild lensing, a source close to the optical axis behind the lens is close to all the odd caustic points and all images are simultaneously enhanced. In Kerr lensing, the caustic points move off the optical axis and are distributed all over the trigonometric interval. For this reason, in general we can have only one enhanced image at a time.

We can specify the magnification formula for the enhanced images using Eq. (86)

$$\mu_k^{enh} = \frac{(D_{OL} + D_{LS})^2}{D_{OL}^2 D_{LS}^2} \frac{\bar{f}'_k(a)}{j_k j}; \quad (88)$$

$$\bar{f}'_k(a) = \frac{\bar{u}(\theta_k(a)) u_m(a) e_k(a)}{\bar{a} \theta_k(a)}; \quad (89)$$

The quantity  $\bar{f}'_k$  regulates the magnification close to caustic points. The dependence on  $a$  has been extracted and has the typical  $j_k j_k^{-1}$  behaviour. The dependence on the astronomical distances  $D_{OL}, D_{LS}, D_{OS}$  of  $\bar{f}'_k$  is negligible at the lowest order in  $\frac{u}{D_{OL}}$ . So we can use  $\bar{f}'_k$  as a measure of the magnifying power of the black hole for different enhanced images and different angular momenta.

In Fig. 7 we plot the magnifying power  $\mu_3$  of the caustic point  $\theta_3$ , which for  $a = 0$  generates the first relativistic image of a source behind the lens. The magnification decreases for negative angular momenta while grows for positive  $a$ . However, when photons start to enter the ergosphere, the magnification rapidly falls down. This is a direct consequence of the analogous behaviour of the coefficients of the strong field limit analyzed in Sect. III. The maximum is slightly anticipated with respect to  $a_{cr}$ , because  $\theta_3$  is pushed forward at high  $a$  and  $e_3$  falls down earlier. Moreover, the images become more packed in this situation. The maximum magnification is achieved at  $a' \approx 0.3$  where we can gain a factor of the order 2 with respect to Schwarzschild lensing. In practice this means

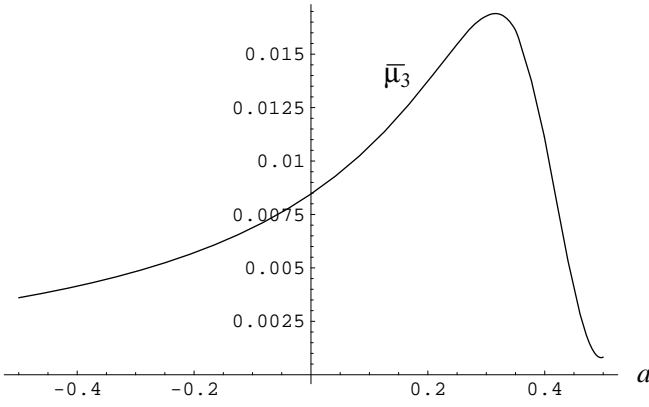


FIG. 7: The magnifying power at the caustic point  $\bar{\mu}_3$ .

that with a source at the same distance from the caustic point, a Kerr black hole with  $a' = 0.3$  magnifies twice more than the corresponding Schwarzschild black hole.

The shape of  $\bar{\mu}_k$  remains more or less the same for every  $k$  but roughly we have that

$$\frac{k+1}{k}, e = 0.043: \quad (90)$$

The magnification of enhanced images falls quite rapidly as we let the photons make more and more loops.

#### A. Critical curves and caustics

It is well known that the Jacobian of the Schwarzschild lens has an infinite series of Einstein rings [3, 5]. The first Einstein ring is the classical weak field Einstein ring whose angular radius is

$$r_E = \frac{r \sqrt{2D_{LS}}}{D_{OL}D_{OS}}: \quad (91)$$

Outside the Einstein ring the Jacobian is positive and we have positive parity images. Inside the Einstein ring we have negative parity images. The corresponding caustic is the point at  $\beta_1 = 0$ .

At small impact parameters we enter the strong field limit of the Schwarzschild lensing and the light rays wind around the black hole. The second Einstein ring is created by photons coming back towards the observer. Inside this second Einstein ring the Jacobian returns positive. The caustic is at  $\beta_2 = 0$ .

Decreasing  $u$  further, the light ray completes a loop and we have the third Einstein ring, whose caustic point is  $\beta_3 = 2$  and is superposed on the first caustic point (on the second Riemann fold). Inside this Einstein ring the Jacobian returns negative.

The Schwarzschild lensing and its extension to spherically symmetric metrics analyzed in Refs. [5, 8, 9, 10, 11] considered a source behind the black hole, hence close to the odd caustic points. In this situation, both  $n$ -th relativistic images are formed close to the  $(2n+1)$ -th Einstein

ring. For each  $n$ , the  $n$ -th image on the same side of the source is outside the Einstein ring and is positive, the image on the opposite side is inside the Einstein ring and is negative.

What changes when we turn on the spin of the black hole? As regards the first Einstein ring of the weak limit, it is distorted and shifted and the caustic point turns into a finite extension diamond shaped caustic [19].

As regards the critical curves in the strong field limit, their intersections with the equatorial plane are

$$r_k^{cr}, \theta_k^{cr} = 1 - \frac{u_m e_k (D_{OL} + D_{LS})}{a D_{OL} D_{LS}} \quad (92)$$

$$\theta_k^{cr} = \frac{u_m}{D_{OL}} (1 + e_k): \quad (93)$$

They are closer to the optical axis on the positive  $a$  side (for left-winding photons) and farther on the negative  $a$  side (i.e. for right-winding photons). Therefore critical curves are distorted and shifted towards the negative  $a$  side, that is the western side, if north is the direction of the spin.

The caustics are no longer points but acquire a non vanishing extension.  $r_k(\beta_j)$  and  $\theta_k(\beta_j)$  represent the intersections of the  $k$ -th caustic with the equatorial plane. As  $j_k(\beta_j) < k$  and  $j_k(\beta_j) > k$  the caustic is shifted towards the western side. From Fig. 6 we notice that at high angular momenta the caustics may become very large, covering even several Riemann folds! At the lowest order in  $a$  and neglecting any backreaction on the equatorial lens equation it is impossible to give a detailed classification of the kind of catastrophes we encounter on the equatorial plane. However, the fact that the first caustic in the weak field assumes the typical diamond shape of quadrupole lenses suggests a similar picture for strong field caustics. If this is the case, then the caustic points  $\beta_k$  on the equatorial plane are cusps. This is consistent with the fact that if we let  $a$  decrease below some  $k$  the corresponding image changes parity. This can happen only when at the critical point two images are formed with the same parity of the original image [20, 21]. These images rapidly move in the vertical direction and are missed in our quasi-equatorial approximation.

## VIII. SUMMARY AND DISCUSSION

The modifications to strong field limit gravitational lensing induced by the rotation of the central body are indeed of considerable entity. The most apparent is the formation of extended caustics which, for high angular momenta, can cover several Riemann folds. This situation is radically different from spherically symmetric black holes where the caustics are points aligned behind and in front of the lens. While for  $a = 0$  a source behind the lens is simultaneously close to all odd caustics and gives rise only to enhanced images, for Kerr black holes the source can be close to one caustic at a time and thus

produces only one enhanced image. (To be more precise, the number of caustics is infinite and, at least in principle, the set of  $\chi$  is dense in the trigonometric interval. Therefore every source is close to an infinite subset of caustics, but it must be kept in mind that only the first relativistic caustics yield images significantly amplified for observations).

On the equatorial plane the magnifying power of the caustics is of the same order as that of the Schwarzschild caustic, but for photons winding in the same sense of the black hole (left-winding) a factor 2 can be gained. Not enhanced images are always quasi-equatorial but have very low magnification and can be neglected in observations.

The asymmetry between left-winding and right-winding light rays is reflected on the images: the first are closer to the optical axis and the second are farther and more packed. Left-winding photons spend some time inside the ergosphere if  $a > a_{cr}$ . In this case the images become more packed and the magnification falls down.

The study of quasi-equatorial Kerr gravitational lensing is very instructive and has allowed us to discover a great number of interesting features of spinning black holes. However, before addressing the phenomenology of the black hole at the center of our Galaxy and/or other

black holes, further investigation is necessary. In fact, at least we need a punctual description of the caustic structure not limited to the equatorial plane. Moreover, the existence of extended caustics suggests the formation of pairs of non-equatorial images which are missed in our approximation but could be relevant for the phenomenology. The quasi-equatorial lensing, studied in this work, must be considered as a first fundamental step to understand lensing by spinning black holes, but is not the final one. The complexity of the problem requires a global approach in order to give correct and complete answers to all observational questions. This settles as the main objective for future work on strong field gravitational lensing.

#### Acknowledgments

I am grateful to Mauro Sereno for useful discussions on the subject.

This work is supported by Museo Storico della Fisica e Centro Studi e Ricerche "Enrico Fermi".

- 
- [1] J.M. Bardeen, Black Holes, ed. C. de Witt & B.S. de Witt, NY, Gordon & Breach, 215 (1973).
  - [2] S.J. Viergutz, *A & A* 272 (1993) 355.
  - [3] R.J. Nemiro, *Amer. Jour. Phys.* 61 (1993) 619.
  - [4] H. Falcke, F. Melia, E. Agol, *ApJ Letters* 528 (1999) L13.
  - [5] K.S. Virbhadra, G.F.R. Ellis, *Phys. Rev. D* 62 (2000) 084003.
  - [6] S. Frittelli, T.P. Kling, E.T. Newman, *Phys. Rev. D* 61 (2000) 064021
  - [7] K.S. Virbhadra, G.F.R. Ellis, *Phys. Rev. D* 65 (2002) 103004.
  - [8] V. Bozza, S. Capozziello, G. Iovane & G. Scarpetta, *Gen. Rel. and Grav.* 33 (2001) 1535.
  - [9] E.F. Eiroa, G.E. Romero, D.F. Torres, *Phys. Rev. D* 66 (2002) 024010.
  - [10] A.O. Petters, *astro-ph/0208500*.
  - [11] V. Bozza, *gr-qc/0208075*, to appear on *Phys. Rev. D*.
  - [12] Constellation-X web page: [constellation.gsfc.nasa.gov](http://constellation.gsfc.nasa.gov); Maxim web page: [maxim.gsfc.nasa.gov](http://maxim.gsfc.nasa.gov); J.S. Ulvestad *astro-ph/9901374*.
  - [13] D. Richstone et al., *Nature*, 395 (1998) A14.
  - [14] S. Liu, F. Melia, *ApJ Letters* 573 (2002) 23.
  - [15] R.H. Boyer, R.W. Lindquist, *Jour. of Math. Phys.* 8 (1967) 265.
  - [16] B. Carter, *Phys. Rev.* 174 (1968) 1559.
  - [17] S.W. Hawking, G.F. Ellis, *The large scale structure of space-time*, Cambridge University Press, 1973.
  - [18] C.M. Claudel, K.S. Virbhadra, G.F.R. Ellis, *J. Math. Phys.* 42 (2001) 818.
  - [19] M. Sereno, 2003, in preparation.
  - [20] P. Schneider, A. Wei, *A & A* 260 (1992) 1.
  - [21] S.H. Rhie, *astro-ph/0207612*.